Bioelectrocatalytic hydrogels from electron-conducting metallopolypeptides coassembled with bifunctional enzymatic building blocks

Ian R. Wheeldon*, Joshua W. Gallaway*, Scott Calabrese Barton†, and Scott Banta*‡

*Department of Chemical Engineering, Columbia University, 500 West 120th Street, New York, NY 10027; and †Department of Chemical Engineering and Materials Science, Michigan State University, 1262 Engineering Building, East Lansing, MI 48824-1226

Edited by Robert Langer, Massachusetts Institute of Technology, Cambridge, MA, and approved August 12, 2008 (received for review May 29, 2008)

Here, we present two bifunctional protein building blocks that coassemble to form a bioelectrocatalytic hydrogel that catalyzes the reduction of dioxygen to water. One building block, a metallopolypeptide based on a previously designed triblock polypeptide, is electron-conducting. A second building block is a chimera of artificial α-helical leucine zipper and random coil domains fused to a polyphenol oxidase, small laccase (SLAC). The metallopolypeptide has a helix–random-helix secondary structure and forms a hydrogel via tetrameric coiled coils. The helical and random domains are identical to those fused to the polyphenol oxidase. Electron-conducting functionality is derived from the divalent attachment of an osmium bis-bipyrdine complex to histidine residues within the peptide. Attachment of the osmium moiety is demonstrated by mass spectroscopy (MS-MALDI-TOF) and cyclic voltammetry. The structure and function of the α-helical domains are confirmed by circular dichroism spectroscopy and by rheological measurements. The metallopolypeptide shows the ability to make electrical contact to a solid-state electrode and to the redox centers of modified SLAC. Neat samples of the modified SLAC form hydrogels, indicating that the fused α-helical domain functions as a physical cross-linker. The fusion does not disrupt dimer formation, a necessity for catalytic activity. Mixtures of the two building blocks coassemble to form a continuous supramolecular hydrogel that, when polarized, generates a catalytic current in the presence of oxygen. The specific application of the system is a biofuel cell cathode, but this protein-engineering approach to advanced functional hydrogel design is general and broadly applicable to biocatalytic, biosensing, and tissue-engineering applications.

biocatalysis | biofuel cell | biomaterial | laccase | protein

Protein engineering provides the tool set to design and produce peptides and proteins that form the building blocks of new bio-inspired materials. The tool set allows for the manipulation of natural and artificial DNA sequences encoding the peptides or proteins of interest, and the subsequent biological production of the translated products. The methodology is powerful in that it allows for exact control over the identity and sequence of each residue and, consequently, the structural folding patterns of the resultant peptides or proteins (1). And, just as function stems from structure, it is also controlled within the protein-engineering scheme of materials design. There are a number of successful examples of hydrogels designed for tissue-engineering and drug-delivery applications that use functional protein domains to obtain structural responsiveness to environmental cues (2–4). These examples include responsiveness to pH (5), temperature (6), shear stress (7), and ligand binding (8, 9) among others (refs. 2 and 10; ref. 3 and references therein). A wider range of applications, such as bioelectrocatalysis and biosensing, will benefit from the advantages of protein-based materials design provided that a second functionality, like catalytic activity or electron conduction, can be engineered into the biologically inspired building blocks. It is here that our current interests lie; the development of multifunctional proteins that self-assemble into supramolecular structures and have bioelectrocatalytic functionality.

In the past decade, important advancements have been made in the development of bioelectrocatalysis for biosensing and biofuel cell applications (11, 12). In particular, much success has been achieved with systems that couple biological recognition with an electrochemical signal by electrically connecting the redox active centers of oxidoreductases with a solid-state electrode (11, 13, 14). The most advanced systems are synthetic redox polymer-enzyme hydrogels (15, 16). The redox polymer is often poly(vinyl)pyridine or poly(vinyl)imidazole (PVI) with pendent osmium moieties complexed to a fraction of the nitrogen-containing aromatic rings (14–17). Osmium complexes are used as electron mediators because the redox potential can be tailored to a desired value through ligand substitution, and the complexes are more photostable than other transition metal complexes such as those based on ruthenium (17). Osmium metal and most compounds are generally considered nontoxic (17), although the tetroxide (not used in this work) is highly toxic in cases of acute exposure. The toxicological properties of the salts used here have not been evaluated.

Although much work has been focused on optimizing electron diffusion within the redox polymer-enzyme hydrogels and on improving catalytic performance, little work has been done in evaluating the nano- and microscale structure of these hybrid materials. In general, enzymes are nonspecifically entrapped within the hydrogels by electrostatic interactions, and high loadings of redox moieties are required to ensure electrical contact to the immobilized enzymes (14, 15). There is also evidence that other similar synthetic polymer-enzyme hydrogels are inherently heterogeneous in structure and activity (18–20).

Here, we propose a bioelectrocatalytic hydrogel constructed from bifunctional protein building blocks. Mixtures of electron-conducting and catalytic building blocks will self-assemble into a bioelectrocatalytic supramolecular hydrogel. The physical properties and bulk function of the hydrogel can be independently tuned, because those properties depend on the identity and amount of each building block. The building blocks are based on a previously designed triblock polypeptide, here termed HSH, composed of two α-helical leucine zipper domains (H domain) separated by a randomly coiled domain (S domain) (5, 21). The helical domains assemble into tetramic coiled coils, thus forming an ordered supramolecular hydrogel. Catalytic functionality is derived from an

Author contributions: I.R.W., J.W.G., S.C.B., and S.B. designed research; I.R.W. and J.W.G. performed research; I.R.W., J.W.G., S.C.B., and S.B. analyzed data; and I.R.W. and S.B. wrote the paper.

The authors declare no conflict of interest.

This article is a PNAS Direct Submission.

‡To whom correspondence should be addressed. E-mail: sbanta@cheme.columbia.edu.

This article contains supporting information online at www.pnas.org/cgi/content/full/0805249105/DCSupplemental.

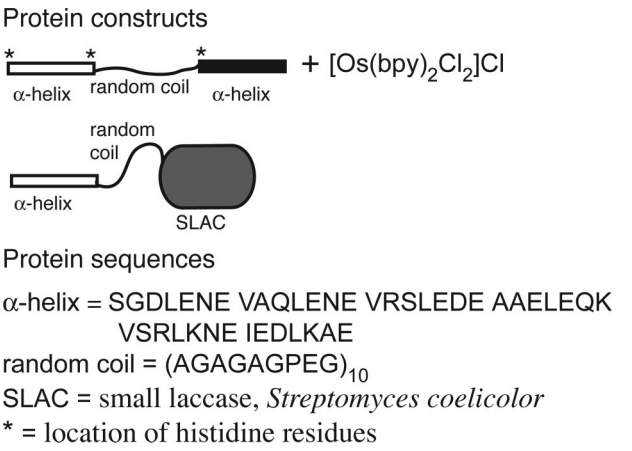

Fig. 1. Protein constructs with partial sequences, and the osmium redox species used in this study.

oxidoreductase to which H domains, identical to those of the triblock polypeptide (HSH), have been genetically fused. Electron conduction functionality is achieved through modification of the HSH building block with a redox moiety.

We explore this class of multifunctional hydrogels by creating a bioelectrocatalytic system that catalyzes the reduction of dioxygen to water at neutral pH, which has proven difficult with synthetic redox–polymer systems. A polyphenol oxidase from *Streptomyces coelicolor* catalyzes the oxidation of a wide range of substrates along with the concomitant reduction of dioxygen to water (22), and it is here used as the basis of the enzymatic building block. The scheme of attaching osmium redox moieties to PVI is an opportune starting point to begin adding electron-conducting functionality to the system, through attachment to the imidazole side chain of histidine residues within the hydrogel forming polypeptide. When coassembled, the two protein building blocks produce a hydrogel that can be used as an electrode surface modification for a cathode in a biofuel cell or as an oxygen biosensor. Thus, we demonstrate that the design and the coassembly of bifunctional protein building blocks constitute a general protein-engineering method for the creation of multifunctional biomaterials.

Results and Discussion

The bioelectrocatalytic hydrogel is made from two compatible building blocks, an engineered bifunctional metallopolypeptide that self-assembles into a hydrogel and is electron conducting, and a polyphenol oxidase, modified with an N-terminal α-helical domain (H domain), that is enzymatic and self-assembles into a supramolecular network. Both the metallopolypeptide and modified polyphenol oxidase are bifunctional in that they exhibit two distinct functionalities. Physical cross-linking functionality of the metallopolypeptide is derived from the previously developed triblock polypeptide, HSH, that forms a supramolecular hydrogel because of the coiled-coil formation of α-helical leucine zipper domains (5). A second functionality, electron conduction, is derived from the divalent attachment of osmium bis-bipyridine via ligand exchange (14–17) with suitable amino acid side chains. The modified polyphenol oxidase, a small laccase (SLAC) (22), was genetically engineered to exhibit physical cross-linking functionality through the addition of the H and S domain encoding sequences to the N terminus of the gene. The protein constructs, relevant amino acid sequences, and the osmium bis-bipyridine complex are shown in Fig. 1. Of specific importance is the location of histidine residues within HSH because the imidazole side chains are the putative location of osmium attachment. N-terminal to the first H domain is a 6× histidine tag. There are also two single histidines, one within each of the linker regions, N- and C-terminal to the S domain. The full amino acid sequence is provided in the supporting information (SI) *Text*.

The attachment procedure of osmium bis-bipyridine to HSH is uncomplicated. A 20:1 molar ratio of osmium to purified HSH was dissolved in deionized water and heated to 70°C under argon, while refluxing. Two metallopolypeptide products were synthesized, OsHSH-1 and OsHSH-2, from reactions lasting 6 and 18 h, respectively. Both products are purple. Reaction for 6 h yields a polypeptide product that migrates on a polyacrylamide gel under denaturing conditions to a distance equivalent to that of HSH (Fig. 2*A*). The product also contains polypeptides that migrate to twice the molecular weight of a single HSH monomer as well as a smearing of material between 90,000 and 120,000. The diffuse bands are dimers, trimers, and tetramers of HSH cross-linked with osmium complex that have undergone two ligand substitutions.

The M_r of HSH as measured by mass spectrometry (MS MALDI-TOF) is 22,050, but it is retarded in the electrophoretic gel to an apparent M_r of 32,000. The same electrophoretic behavior is seen with monomers of OsHSH-1 as MS MALDI-TOF analysis reveals a species with a M_r of 22,060 with two additional broad peaks at 22,570 and 23,080 (Fig. S1). The M_r of an attached osmium bis-bypridine complex is 502.6, 538.1, or 573.5, depending on the number of chloro ligands and ionic chlorides associated with the complex, suggesting that OsHSH-1 is a mixed population of un-

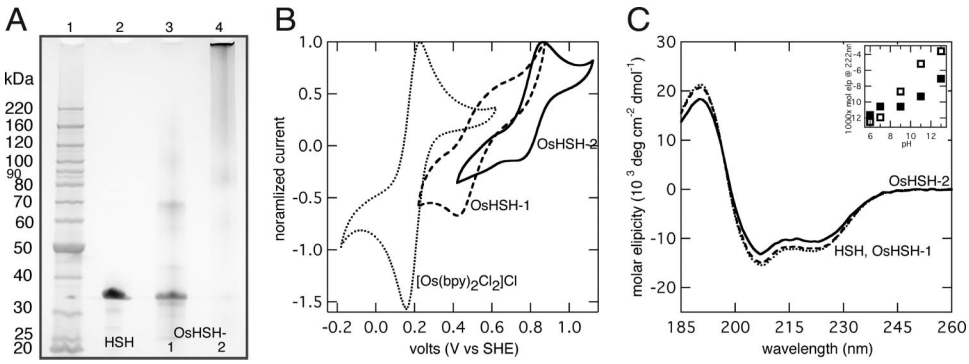

Fig. 2. Characterization of $[Os(bpy)_2Cl_2]Cl$ + HSH synthesis products. (*A*) 4–12% Bis-Tris SDS/PAGE. Lane 1, protein standards; lane 2, unmodified HSH; lane 3, Os-HSH-1; and lane 4, Os-HSH-2. (*B*) Cyclic voltammograms of 10 mg·ml^{-1} $[Os(bpy)_2Cl_2]Cl$, 35 mg·ml^{-1} Os-HSH-1, and 35 mg·ml^{-1} Os-HSH-2 in quiescent solution, 100 mV·s^{-1}, 100 mM Na_iP, pH 7.0. The voltammograms are normalized to 1.0 based on the maximum current density, i_{max}. i_{max} values (in μA cm^{-2}) are: $[Os(bpy)_2Cl_2]Cl$, 5.3; OsHSH-1, 1.3; OsHSH-2, 62. (*C*) CD spectra of 5 μM samples in 10 mM Na_iP, pH 7, at 22°C. (*Inset*) Mean residue ellipticity of Os-HSH-1 (open) and OsHSH-2 (closed) at pH 6–13. (*B* and *C*) Os-HSH-1 (dashed) and Os-HSH-2 (solid); (*B*) $[Os(bpy)_2Cl_2]Cl$ (dots) and (*C*) HSH (dots).

modified HSH, HSH with a single osmium complex, and HSH to which two complexes have been bound.

After reaction for 18 h, the majority of the polypeptide product OsHSH-2 appears to be highly polymerized, based on limited migration of product into the gel (Fig. 2*A*). A smear of protein appears at a M_r of 120,000 and larger, as well as smaller diffuse bands at ≈90,000 and 60,000 and a faint band at 32,000. Similar to OsHSH-1, the higher molecular weight species are multimers of osmium-modified HSH. The high degree of multimerization seen in OsHSH-2 suggests that it no longer functions as a monomeric (or dimeric, or trimeric) building block in a supramolecular hydrogel, but more likely, will function as a chemically cross-linked high-molecular-weight hydrogel. It is included here as evidence of osmium bis-bipyridine ligand substitution and as it is a distinct, viable product in and of itself.

The standard redox potential, $E°$, of the osmium complex depends on the identity of each ligand and, as such, can be tailored to a desired value (17). Ligand substitution can also be confirmed by measurement of a shift in redox potential. Substitution of a chloride ligand of $[Os(bpy)_2Cl_2]Cl$ by imidazole or poly(*N*-vinylimidazole) shifts $E°$ from 190 mV vs. standard hydrogel electrode (SHE) to 400–470 mV; substitution of the second chloride results in a further shift in $E°$ to 710–850 mV (15). The major voltammetric peaks of OsHSH-1 and OsHSH-2 in dilute solution are centered at potentials of 470 and 800 mV, respectively (Fig. 2*B*). Minor peaks are also observed at 800 mV for OsHSH-1 and 470 mV for OsHSH-2, but in light of the *a priori* estimates of potential shifts resulting from ligand exchange, reaction for 6 h results predominately in a single ligand substitution of chloride by an imidazole side chain of a histidine residue. At longer reaction times, a second chloride ligand is exchanged. The assertion that $[Os(bpy)_2Cl_2]Cl$ undergoes a second ligand exchange is supported by the apparent multimerization of OsHSH-2; the complex acts as a cross-link between hydrogel monomers at one residue per polypeptide resulting in a chemically cross-linked network of high molecular weight.

MS MALDI-TOF analysis of protease-digested samples of OsHSH-1 also supports the proposed ligand exchange. Five fragments seen in trypsinized samples of OsHSH-1 are not observed in similarly treated HSH and correspond to the molecular weight of an expected histidine-containing peptide fragment plus an osmium bis-bipyridine complex with zero, one, or two chlorides (Table S1). The same is true of four fragments seen in AspN-digested samples (Table S1).

Physical cross-linking of HSH into a supramolecular hydrogel is mediated by the agglomeration of the H domains into coiled-coil bundles, thus secondary structure is essential to hydrogel functionality. Circular dichroism (CD) spectroscopy of OsHSH-1 and OsHSH-2 indicates that the secondary structure is not compromised as evidenced by the spectral minima at 208 and 222 nm, characteristics of α-helices (23) (Fig. 1*C*). Deconvolution of the spectra by using the Johnson and Hennessey method (24) shows that there is no statistical difference between the helical content of OsHSH-1 and HSH (36.3 ± 2.2% and 36.2 ± 2.4%, respectively; $n = 5$, $P = 0.979$) and only a slight, but statistically relevant, decrease in OsHSH-2 (32.2 ± 2.0%; $n = 5$, $P = 0.0199$). Additionally, both osmium-modified polypeptides retain the designed pH-dependent structure (5) as seen in the loss of helical content with increasing pH (Fig. 2*C Inset*).

Rheological experiments show that on rehydration in aqueous solution buffered to pH 7.0, 7.5 wt% samples of OsHSH-1 and OsHSH-2 form hydrogels. In small amplitude oscillatory shear experiments both OsHSH-1 and OsHSH-2 exhibit storage modulus, G′, plateau values consistently greater than the elastic modulus, G″, a characteristic indicative of hydrogel formation (25). A 7.5 wt% sample of OsHSH-1 at pH 7.0 and 22°C exhibits a G′ plateau value of 380 ± 70 Pa, and a similar sample of OsHSH-2 has a G′ of 640 ± 40 Pa. In comparison, a 7.5 wt% sample of HSH at pH 7.0 has a G′ of 560 ± 130 Pa (26). The G″ values of all samples reach plateaus <100 Pa. The lower phase transition limit was not rigorously studied, but hydrogel formation of OsHSH-1 and OsHSH-2 was visually confirmed at concentrations as low as 6.0 wt%; the samples did not appear to flow or deform under gravity on a timescale of tens of hours.

The function of the H domains is also confirmed by the formation of hydrogels of OsHSH-1 through a change in pH from highly basic to near-neutral. At pH 12, secondary structure is lost and OsHSH-1 does not form a hydrogel, but at pH 7 the metallopolypeptide regains secondary structure and physical cross-linking functionality. Five-microliter samples of 7.5 wt% OsHSH-1 at pH 12 were aliquoted on to glassy carbon electrodes and dried overnight. Hydrogels were formed on rehydration at neutral pH. OsHSH-2 does not exhibit the same functional pH dependence, because 7.5 wt% samples at pH 12 do form hydrogels regardless of the loss of secondary structure. Examples of a 7.5 wt% OsHSH-1 hydrogel at pH 7 and solution of the same concentration at pH 12 are shown in Fig. 3*A*.

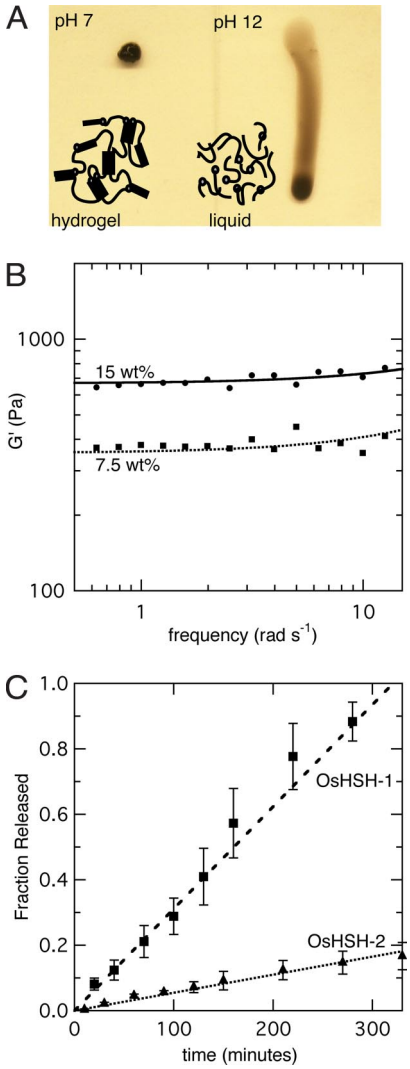

Fig. 3. Characterization of OsHSH hydrogels. (*A*) Picture of 7.5 wt% samples of OsHSH-1 on a vertical glass slide at pH 7.0 (*Left*) and pH 12 (*Right*). The picture was taken immediately after standing the glass side on edge. (*B*) Small-amplitude oscillatory shear experiments of 7.5 (squares) and 15 wt% (circles) sample of OsHSH-1, 100 mM NaiP, pH 7, 22°C. (*C*) Fractional release of 7.5 wt% samples of OsHSH-1 (squares) and OsHSH-2 (triangles) into quiescent open buffer solution, 100 mM Na_iP, pH 7.0, at 25°C.

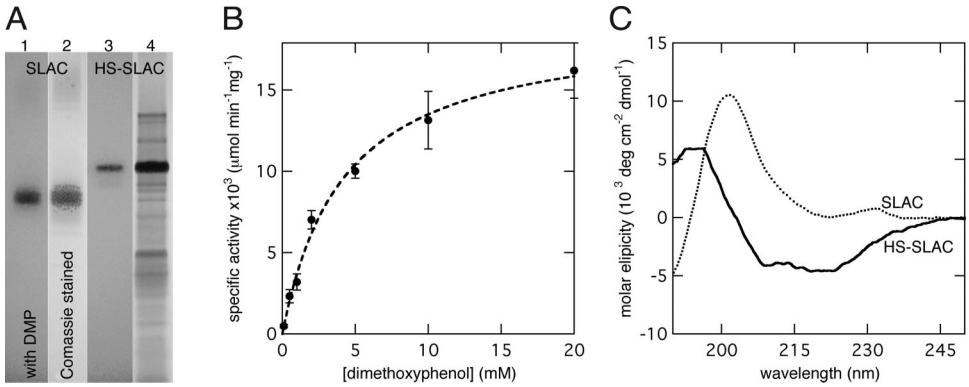

Fig. 4. Characterization of HS-SLAC. (*A*) In-gel activity assay of SLAC and HS-SLAC in a 16% tricene native gel. SLAC washed with 30 mM DMP (lane 1) and Coomassie blue stained (lane 2). HS-SLAC washed with 30 mM DMP (lane 3), and Coomassie blue stained (lane 4). (*B*) Dilute solution activity of HS-SLAC with DMP and air-saturated solution, 10 mM Na_iP, pH 7.0, at 25°C. (*C*) CD spectra of SLAC (dots) and HS-SLAC (solid) at pH 7.0.

Hydrogel strength, in terms of G′, can be increased with the addition of building blocks as this increases the helical cross-linking concentration. A 15 wt% sample of OsHSH-1 shows an increase in G′ to 950 ± 170 Pa (Fig. 3*b*). We have previously shown that building blocks with compatible helices form macrohomogeneous mixed hydrogels (26). Therefore, by mixing HSH with OsHSH-1 it is possible to independently tune hydrogel strength and osmium concentration by varying the amounts and ratio of HSH to OsHSH-1.

The high degree of multimerization seen in OsHSH-2 contributes substantially to the overall cross-linking of the network, but physical cross-linking due to coiled-coil formation is still thought to occur. A decrease in the ratio of CD signal at 222 and 208 nm from 0.84 to 0.78, under native conditions compared with samples in 50% trifluoroethanol (TFE), a compound that is known to disrupt coiled-coil formation, suggests that OsHSH-2 forms coiled coils (27). A similar decrease in the signal ratio is observed with HSH. The typical ratios of ellipticity at 222 to 208 nm for coiled coils, 1.0, and single helices, 0.8 (27), are not strictly applicable in this case because the polypeptides are only 32–36% helical. The random coil domain (S domain) separating the helices contributes to the negative dichroic signal between 210 and 195 nm (23) decreasing the expected signal ratio of 222 to 208 nm. We point to the change in signal ratios of both HSH and OsHSH-2 as support for the change in tertiary structure under native and coil-disruptive conditions.

It has been shown that the predominate mechanism of erosion of HSH hydrogels is diffusion of small-number closed-loop complexes formed via strand exchanged between coiled coils (28). When a closed-loop forms at the surface of the hydrogel it can diffuse into open buffer solution on a timescale faster than reattachment to the greater network via a subsequent strand exchange. With the additional cross-linking due to the osmium modification, erosion rate is suppressed as closed-loop formation is impeded, or, at least, the number of monomers required for closed-loop formation is increased. HSH is completely eroded after 180 min (28). After 5.5 h OsHSH-1 is >95% eroded and OsHSH-2 is only17 ± 4% eroded (Fig. 3*C*). Erosion rate can be further suppressed by treating rehydrated hydrogels with glutaraldehyde, thus further preventing closed-loop formation. Chemical cross-linking between amine groups results in near-complete suppression of erosion after 5 min of treatment with 1% glutaraldehyde solution (Fig. S2). Effects of glutaraldehyde cross-linking on the nano- and microstructure of the supramolecular network have not yet been studied. Additionally, nonspecific chemical cross-linking could have an effect on the electron diffusion coefficient within OsHSH-1 hydrogels and on the catalytic properties of enzymes within an OsHSH-1 hydrogel. Other strategies for controlling the erosion rate of coiled-coil cross-links have been studied elsewhere (26, 28).

Electron-conducting functionality of the metallopolypeptide hydrogels is best demonstrated through the intended application, the bioelectrocatalyic reduction of dioxygen to water. To do so, a second building block, one that coassembles with OsHSH-1 into supramolecular hydrogel and exhibits catalytic activity toward the reduction of dioxygen to water, is required. We have recently shown that the H and S domains of HSH can be appended to the termini of fluorescent proteins without disrupting native structure and function, suggesting that a catalytic building block could be made via a similar design (26). Because SLAC has been shown to be active at neutral pH in the presence of osmium bis-bipyridine (29) it is an ideal candidate for the catalytic building block. The sequences encoding the H and S domains were ligated to the N terminus of the SLAC gene and the chimeric protein construct, HS-SLAC, was expressed.

In the initial work characterizing SLAC, Machczynski *et al.* (22) demonstrate that dimer formation is required for catalysis; this is also the case with HS-SLAC. Eluate from nickel-affinity chromatography purified HS-SLAC contains putative monomers and dimers, but only the higher-molecular-weight protein (the putative dimers) exhibit catalytic activity in a native in-gel activity assay (Fig. 4*A*). The active band in the native gel corresponds to a protein that runs on a denaturing gel to an apparent M_r between 120,000 and 160,000 (Fig. S3). The calculated M_r of the HS-SLAC dimer is 97,398, but in light of the electrophoretic behavior of HSH and OsHSH-1, the high apparent M_r is not unexpected. Unmodified SLAC dimers were used as a positive control, and as the wild-type SLAC also exhibits in-gel activity with 30 mM dimethoxyphenol (DMP) in air-saturated solution at pH 7.0.

Further characterization of HS-SLAC dimers with dilute solution activity assays reveals an apparent Michaelis–Menton constant, K_M, toward DMP in air-saturated solution of 4.2 ± 0.5 mM and a k_{cat} of 2 ± 0.1 min^{-1} at pH 7.0 (Fig. 4*B*). Comparison with unmodified SLAC reveals that, although the N-terminal addition of the H and S domains did not prevent dimer formation, catalytic activity is impaired. Under similar conditions (pH 7.2, air-saturated solution and with DMP as cosubstrate) unmodified SLAC exhibits a k_{cat} of 350 min^{-1} and an apparent K_M toward DMP of 4 mM (22).

A bifunctional catalytic building block requires that the structure and function of the cross-linking domains also be intact. CD spectroscopy shows that the appended H domain does have helical secondary structure as evidenced by the introduction of spectra minima at 208 and 222 nm, characteristics of α-helices (Fig. 4*C*). Deconvolution of the SLAC and HS-SLAC spectra

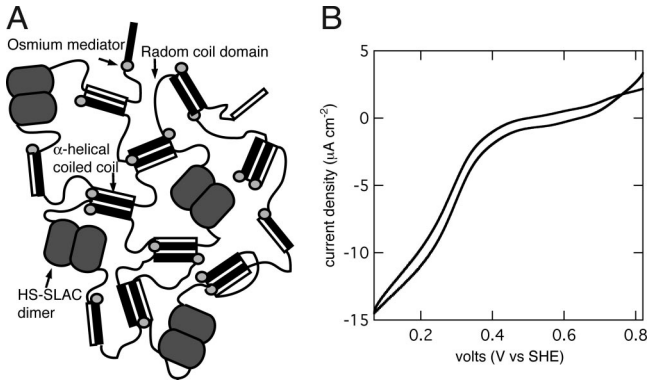

Fig. 5. Bioelectrocatalytic hydrogel. (*A*) Schematic diagram of OsHSH-1 and HS-SLAC supramolecular hydrogel. (*B*) Bioelectrocatalysis of a mixed hydrogel of 7.5 wt% OsHSH-1 and 2.5 wt% HS-SLAC on a 3-mm glassy carbon rotating disk electrode. Buffered to pH 7.0 with 100 mM Na_iP, 900 rpm, 25°C, 1 mM O_2.

with the CDSSTR algorithm (30) suggests an increase in total helical content from 0 to 7.0 ± 1.0%. Cross-linking functionality of the H domain was confirmed by hydrogel formation of a 32 wt% sample of HS-SLAC at pH 7.0. Hydrogel formation was visually confirmed in the same manner as the lower phase transition limit of OsHSH-1 and -2, the sample did not flow or deform under gravity. The exceedingly high concentration of HS-SLAC (320 mg·ml^{-1}) required to attain an equal helical concentration as 7.5 wt% OsHSH-1 was a major impediment to further rheological characterization. Visual confirmation of hydrogel formation, as compared with the non-gel-forming unmodified SLAC at the same concentration and under the same conditions, provides sufficient evidence for physical cross-linking functionality.

Fig. 5*A* is a schematic representation of a mixed hydrogel of OsHSH-1 and HS-SLAC. The active dimers of HS-SLAC are incorporated within the network of OsHSH-1 by means of physical cross-linking at the coiled-coil bundles. Cross-linking within the network occurs by three modes: coiled-coil formation, dimer formation of HS-SLAC, and osmium-mediated cross-linking within OsHSH-1. Cross-linking due to coiled-coil formation in OsHSH-1 and HS-SLAC was demonstrated by hydrogel formation of neat samples of both constructs at pH 7 (Fig. 3*A* and text above). The helical domain fused to the N terminus of HS-SLAC is identical to those of OsHSH-1, and will form coiled coils within the metallopolypeptide network. SLAC is enzymatically active only as a dimer, therefore a catalytically active hydrogel necessarily includes cross-linking due to protein–protein interactions between HS-SLAC monomers (Fig. 4*A*). Third, as seen in the electrophoretic analysis of OsHSH-1 and OsHSH-2 (Fig. 2*A*) the modification of HSH with osmium bis-bipyridine results in the formation of dimers, trimers, and tetramers, which in the supramolecular hydrogel contribute, in part, to the total cross-linking of the network. Although it is experimentally difficult to quantify the cross-linking density of each mode, there is evidence demonstrating the existence of each. In the case of neat OsHSH-1 and HS-SLAC hydrogels it is clear (based on evidence presented above) that coiled-coil formation is the dominant mode; this holds true for mixed hydrogels of OsHSH-1 and HS-SLAC as well.

A mixed hydrogel of 7.5 wt% OsHSH-1 and 2.5 wt% HS-SLAC on glassy carbon in aqueous solution buffered to pH 7.0 with 100 mM Na_iP at 25°C produces a catalytic current of 12.3 ± 5.2 μA·cm^{-2} 15 min after rehydration (Fig. 5*B*). No catalytic current is observable under N_2 sparging, and an osmium-free control of 7.5 wt% HSH and 2.5 wt% HS-SLAC shows no redox activity. Bioelectrocatalysis requires electron transfer within the electrode surface modification, by means of self-exchange between redox moieties and via heterogeneous electron transfer from the redox moieties to the redox centers of immobilized enzymes. The generation of a catalytic current from a mixed OsHSH-1 and HS-SLAC hydrogel demonstrates the ability of OsHSH-1 to fulfill the redox mediator functions. In addition, the catalytic current demonstrates that HS-SLAC maintains enzymatic function while bound within the hydrogel network.

Synthetic redox polymer hydrogels benefit from electrostatic forces to immobilize enzymes within the film, limiting the choice of enzymes to those that are both active and polyanionic at operating conditions. SLAC is active at pH 7.0, but with a pI of 8.4 (22) it is polycationic and therefore not matched to synthetic redox hydrogel systems operating at neutral pH (29). However, a PVI-Os redox polymer-SLAC hydrogel can initially achieve 1.5 mA·cm^{-2} at pH 7.0 and 40°C (29). A similar system with a fungal laccase from *Trametes versicolor* reaches 0.2 mA·cm^{-2} under similar conditions (29). Milliampere per cm^2 current densities have also been demonstrated with bilirubin oxidase from *Trachyderma tsunodae* immobilized in a PVI-Os redox polymer on high-surface-area carbon cloth (31).

Although the protein-based system presented here does not attain the catalytic current densities of the state-of-the-art hybrid systems, it achieves bioelectrocatalysis with much less osmium redox mediator. The upper limit of osmium concentration in a hydrogel can be estimated from the MS MALDI-TOF results of OsHSH-1 presented above. OsHSH-1 is a mixed population of unmodified HSH, HSH with a single osmium complex and HSH to which two complexes have been bound. If we assume that the OsHSH-1 population is composed entirely of HSH with two complexes, the osmium concentration of a 7.5 wt% hydrogel is 6.5 mM, assuming the hydrogels do not swell beyond the volume used to rehydrate the sample (26). A reasonable assumption of the lower limit is 0.5 osmium moieties per HSH or 1.7 mM. The upper limit of osmium concentration is 1.5–2 orders of magnitude less than the 100–500 mM typically found in synthetic redox polymer systems (14). That a catalytic current is produced with such a low osmium concentration suggests that the electron diffusion (via electron transfer between osmium moieties) is efficient and that the apparent electron diffusion coefficient is large. Additionally, as demonstrated above (Fig. 3*B*), the concentration of osmium moieties is easily controlled.

The major redox couple of OsHSH-2 lies at a potential more oxidizing than that of HS-SLAC, indicating that the osmium moieties of OsHSH-2 would not serve as a reducing substrate in this system. Therefore, this configuration was not tested under bioelectrocatalytic conditions. Neat hydrogels of OsHSH-2 do, however, show redox activity in a cyclic voltammogram (Fig. S4).

Conclusions

Here, we have shown that an electrode surface modification made from a metallopolypeptide and an engineered chimeric polyphenol oxidase can support the bioelectrocatalytic reduction of dioxygen to water. The protein building blocks are bifunctional in that they exhibit physical cross-linking functionality in addition to electron transport or enzymatic functionality. The bioelectrocatalytic system presented here is an example of an all-protein-based, self-assembling, electrode surface modification. The bifunctionality of the protein building blocks allows for the functional components of the bioelectrocatalytic system (i.e., the redox mediator and oxidoreductase) to also act as the physical structure of the hydrogel. The modularity of the system allows for the independent tuning of the physical properties and bulk functionality. The system presented here can function as a cathode in a biofuel cell or biosensor as is, but importantly, the design is general and can be applied to other advanced hydrogel applications such as tissue engineering and drug delivery.

Experimental Procedures

Polypeptide Expression and Purification. Plasmid encoding the hydrogel forming polypeptide AC10A(trp), here termed HSH, was a kind gift from D. Tirrell (CalTech). Expression was carried out as previously described (26). In brief, 750 ml of Terrific Broth (TB) media (Sigma) with 200 $\mu g \cdot ml^{-1}$ ampicillin (Sigma) and 50 $\mu g \cdot ml^{-1}$ kanamycin (Sigma) was inoculated with 10 ml of mature SG13009 *Escherichia coli* (Qiagen) containing pQE9AC10Atrp. The culture was induced with 1.5 mM β-D-1-thiogalactopyranodise (IPTG; Promega) at an OD of 0.85–1.05. Expression continued at 37°C for 5 h. HSH was purified by nickel-affinity chromatography (His-Trap Crude, GE Healthcare) to >95% purity as judged by SDS/PAGE. The purified polypeptide was lyophilized after dialysis against water for 3 days.

Construction of pQE9HSslac and Expression and Purification of HS-SLAC. The plasmid pSLAC was a kind gift from G. Canters (Leiden University, The Netherlands). The SLAC gene was extracted from pSLAC by PCR (*SI Text*). The upstream primer adds a unique SphI restriction site and the downstream primer a unique HindIII site. The SLAC gene was ligated into pQE9AC10Acys (also a gift from D. Tirrell) at the unique SphI and HindIII sites. The resulting plasmid, pQE9HSslac, was propagated in a 5α *E. coli* cell line (New England Biolabs), extracted and inserted into the SG13009 expression cell line.

Expression of HS-SLAC was done in 750-ml batches of TB media with 200 $\mu g \cdot ml^{-1}$ and 50 $\mu g \cdot ml^{-1}$ kanamycin inoculated with 10 ml of overnight culture of SG13009 containing pQE9HSslac. Cultures were grown to an OD = 1.4–1.5 at 30°C before induction with 0.5 mM IPTG. Expression continued for 18–20 h at 24°C. Cells were harvested by centrifugation and purified by nickel-affinity gel filtration chromatography. Detailed procedures are given in *SI Text*.

Synthesis of Os-HSH. The osmium complex $[Os(bpy)_2Cl_2]Cl$ was synthesized from K_2OsCl_6 and bipyridine (Fisher Chemical) as described in ref. 15. Purified HSH (20 $mg \cdot ml^{-1}$) in deionized (DI) water was mixed with 10 $mg \cdot ml^{-1}$ $[Os(bpy)_2Cl_2]Cl$ (1:20 molar ratio) and the reaction vessel was immersed in heating oil held to 70°C. The reaction was allowed to proceed for 6–18 h under argon atmosphere and with constant stirring. The synthesis product was filtered over a 10-kDa cellulose filter with 500 times the reaction volume (1 liter) each of DI water and PBS (50 mM Na_iP, 500 mM NaCl). The product was lyophilized after 3 days of dialysis against DI water.

Hydrogel Preparation. Neat hydrogels of OsHSH-1 and OsHSH-2 were prepared by one of two methods: (*i*) rehydrating lyophilized protein with aqueous solution buffered to pH 7.0 with 100 mM Na_iP; (*ii*) aliquots of OsHSH-1 solution at pH 12 were dried in-place and rehydrated in aqueous solution buffered to pH 7.0 with 100 mM Na_iP. Preparation of mixed hydrogels on glassy carbon electrode surface was accomplished by drying ≈3 μl of wet hydrogel on the electrode surface and rehydrating before analysis. The rate of hydrogel erosion was measured as described in ref. 26.

Electrochemical Measurements. All electrochemical measurements were done in a three-electrode experiment with a platinum wire as the counter electrode, a Ag/AgCl reference electrode, and glassy carbon working electrode. Bioelectrocatalytic and dilute solution experiments were done in 100 mM Na_iP, pH 7.0. All measurements were taken by using a μAutoLab potentiostat. Rotating disk electrode (RDE) experiments were conducted with a polished 3-mm glassy carbon RDE. Potentials are stated versus the standard hydrogel electrode (SHE).

Circular Dichroism. Experiments were conducted with a Jasco J-815 spectrometer. Samples at a concentration of ≈5 μM were prepared from lyophilized polypeptide with 10 mM Na_iP buffer of appropriate pH.

Mass Spectroscopy. MS MALDI-TOF analyses of protease-digested and undigested samples were done at the Protein Core Facility at Columbia University by using an Applied Biosystems Voyager DE Pro. Modified and unmodified HSH were digested with Trypsin and AspN (New England Biolabs) for 16 h at 37°C.

Rheology. Small-amplitude oscillatory shear experiments were preformed with a TA Instruments AR1200 constant stress rheometer equipped with an 8-mm steel parallel plate with the gap of 500 μm, a constant strain of 1%, at 22°C. A bead of mineral oil around the edge of the sample was used to prevent dehydration of the hydrogels.

Activity Assays. Activity of HS-SLAC in dilute solution was measured with dimethoxyphenol (DMP) and air-saturated aqueous solution with 10 mM Na_iP, pH 7.0. Oxidation of DMP was monitored at 468 nm, ε = 14,800 $M^{-1}\,cm^{-1}$ as described in ref 22. In-gel activity assays were done in 16% Tricene native gels (Invitrogen). Before fixing and Coomassie blue staining, the gel was washed with 100 mM Na_iP, pH 7.0, for 30 min and incubated with a fresh buffer solution containing 30 mM DMP for an additional 30 min. Activity was confirmed by observing a purple precipitate of oxidized DMP.

ACKNOWLEDGMENTS. We thank D. Tirrell (CalTech) for the kind gift of the expression plasmid pQE9AC10Atrp, G. Canters (Leiden University, The Netherlands) for his gift of pSLAC, and Y. Itagaki for his help with the MS-MALDI experiments. This work was supported by Air Force Office of Scientific Research Multidisciplinary University Research Initiative (FA9550-06-1-0264).

1. van Hest JCM, Tirrell DA (2001) Protein-based materials, toward a new level of structural control. *Chem Comm* 19:1897–1904.
2. Kopecek J (2007) Hydrogel biomaterials: A smart future? *Biomaterials* 28:5185–5192.
3. Ulijn RV, *et al.* (2007) Bioresponsive hydrogels. *Mater Today* 10:40–48.
4. Chockalingam K, Blenner M, Banta S (2007) Design and application of stimulus-responsive peptide systems. *Protein Eng Des Sel* 20:155–161.
5. Petka WA, Harden JL, McGrath KP, Wirtz D, Tirrell DA (1998) Reversible hydrogels from self-assembling artificial proteins. *Science* 281:389–392.
6. Wang C, Stewart RJ, Kopecek J (1999) Hybrid hydrogels assembled from synthetic polymers and coiled-coil protein domains. *Nature* 397:417–420.
7. Haines-Butterick L, *et al.* (2007) Controlling hydrogelation kinetics by peptide design for three-dimensional encapsulation and injectable delivery of cells. *Proc Natl Acad Sci USA* 104:7791–7796.
8. Ehrick JD, *et al.* (2005) Genetically engineered protein in hydrogels tailors stimuli-responsive characteristics. *Nat Mater* 4:298–302.
9. Murphy WL, Dillmore WS, Modica J, Mrksich M (2007) Dynamic hydrogels: Translating a protein conformational change into macroscopic motion. *Angew Chem Int Ed* 46:3066–3069.
10. Chau Y, *et al.* (2008) Incorporation of a matrix metalloproteinase-sensitive substrate into self-assembling peptides—A model for biofunctional scaffolds. *Biomaterials* 29:1713–1719.
11. Newman JD, Setford SJ (2006) Enzymatic biosensors. *Mol Biotechnol* 32:249–268.
12. Bullen RA, Arnot TC, Lakeman JB, Walsh FC (2006) Biofuel cells and their development. *Biosens Bioelectron* 21:2015–2045.
13. Ikeda T, Kano K (2003) Bioelectrocatalysis-based application of quinoproteins and quinoprotein-containing bacterial cells in biosensors and biofuel cells. *Biochim Biophys Acta Proteins Proteomics* 1647:121–126.
14. Heller A (2006) Electron-conducting redox hydrogels: Design, characteristics and synthesis. *Curr Opin Chem Biol* 10:664–672.
15. Gallaway JW, Calabrese Barton S (2008) Kinetics of redox polymer-mediated enzyme electrodes. *J Am Chem Soc* 130:8527–8536.
16. Mano N, Soukharev V, Heller A (2006) A laccase-wiring redox hydrogel for efficient catalysis of O2 electroreduction. *J Phys Chem B* 110:11180–11187.
17. Calabrese Barton S, Gallaway J, Atanassov P (2004) Enzymatic biofuel cells for Implantable and microscale devices. *Chem Rev* 104:4867–4886.
18. Bartlett PN, Cooper JM (1993) A review of the immobilization of enzymes in electropolymerized films. *J Electroanal Chem* 362:1–12.
19. Maciejewska M, Schafer D, Schuhmann W (2006) SECM imaging of spatial variability in biosensor architectures. *Electrochem Commun* 8:1119–1124.
20. Iwasaki Y, *et al.* (2002) Imaging of electrochemical enzyme sensor on gold electrode using surface plasmon resonance. *Biosens Bioelectron* 17:783–788.
21. Shen W, Lammertink RGH, Sakata JK, Kornfield JA, Tirrell DA (2005) Assembly of an artificial protein hydrogel through leucine zipper aggregation and disulfide bond formation. *Macromolecules* 38:3909–3916.
22. Machczynski MC, Vijgenboom E, Samyn B, Canters GW (2004) Characterization of SLAC: A small laccase from Streptomyces coelicolor with unprecedented activity. *Protein Sci* 13:2388–2397.
23. Johnson WC (1990) Protein secondary structure and circular dichroism—A practical guide. *Protein Struct Funct Genet* 7:205–214.
24. Hennessey JP, Johnson WC (1981) Information content in the circular dichroism of proteins. *Biochemistry* 20:1085–1094.
25. Kavanagh GM, Ross-Murphy SB (1998) Rheological characterisation of polymer gels. *Progr Polymer Sci* 23:533–562.
26. Wheeldon IR, Barton SC, Banta S (2007) Bioactive proteinaceous hydrogels from designed bifunctional building blocks. *Biomacromolecules* 8:2990–2994.
27. Lau SYM, Taneja AK, Hodges RS (1984) Synthesis of a model protein of defined secondary and quaternary structure—Effect of chain-length on the stabilization and formation of 2-stranded alpha-helical coiled-coils. *J Biol Chem* 259:3253–3261.
28. Shen W, Zhang KC, Kornfield JA, Tirrell DA (2006) Tuning the erosion rate of artificial protein hydrogels through control of network topology. *Nat Mater* 5:153–158.
29. Gallaway J, *et al.* (2008) Oxygen-reducing enzyme cathodes produced from SLAC, a small laccase from Streptomyces coelicolor. *Biosens Bioelectron* 23:1229–1235.
30. Sreerama N, Woody RW (2000) Estimation of protein secondary structure from circular dichroism spectra: Comparison of CONTIN, SELCON, and CDSSTR methods with an expanded reference set. *Anal Biochem* 287:252–260.
31. Mano N, Kim HH, Heller A (2002) On the relationship between the characteristics of bilirubin oxidases and O-2 cathodes based on their ''wiring.'' *J Phys Chem B* 106:8842–8848.